



Aerosol-induced changes in sky polarization pattern: potential hint on applications in polarimetric remote sensing

Wei Chen , Shuang Bai , Dexuan Wang , Haimeng Zhao , Hao Sun , Lina Yi , Hengqian Zhao , Donghui Xie , Jouni Peltoniemi & Zhanqing Li

To cite this article: Wei Chen , Shuang Bai , Dexuan Wang , Haimeng Zhao , Hao Sun , Lina Yi , Hengqian Zhao , Donghui Xie , Jouni Peltoniemi & Zhanqing Li (2020) Aerosol-induced changes in sky polarization pattern: potential hint on applications in polarimetric remote sensing, International Journal of Remote Sensing, 41:13, 4963-4980, DOI: [10.1080/01431161.2019.1685724](https://doi.org/10.1080/01431161.2019.1685724)

To link to this article: <https://doi.org/10.1080/01431161.2019.1685724>



© 2019 The Author(s). Published by Informa UK Limited, trading as Taylor & Francis Group.



Published online: 07 Nov 2019.



Submit your article to this journal [↗](#)



Article views: 948



View related articles [↗](#)







View Crossmark data [↗](#)



Citing articles: 3 View citing articles [↗](#)

Aerosol-induced changes in sky polarization pattern: potential hint on applications in polarimetric remote sensing

Wei Chen ^a, Shuang Bai^a, Dexuan Wang^a, Haimeng Zhao^b, Hao Sun ^a, Lina Yi^a, Hengqian Zhao ^a, Donghui Xie^c, Jouni Peltoniemi ^d and Zhanqing Li^e

^aCollege of Geoscience and Surveying Engineering, China University of Mining & Technology, Beijing, China; ^bKey Laboratory of Unmanned Aerial Vehicle Telemetry, Guilin University of Aerospace Technology, Guilin, China; ^cState Key Lab of Remote Sensing Science, Faculty of Geographical Science, Jointly Sponsored by Beijing Normal University and Institute of Remote Sensing and Digital Earth of Chinese Academy of Sciences, Beijing, China; ^dFinnish Geospatial Research Institute FGI, Masala, Finland; ^eEarth System Science Interdisciplinary Center, University of Maryland, College Park, MD, USA

ABSTRACT



Polarization is the intrinsic property of electromagnetic wave and has not been fully investigated in remote sensing field. The incident solar radiation is polarized by the components in the atmosphere and shows stable patterns. Therefore, the sky polarization could be served as an important information source for navigation. However, how different factors affecting the variations of sky polarization pattern is still a complex question, making it difficult to apply sky polarization pattern in navigation. Aerosol is one of the major sources for this uncertainty. Current studies mainly neglect aerosol or just consider aerosol optical depth (AOD), without considering microphysical properties of aerosol. In this study, we perform the influences of both aerosol mode and AOD on the trends of sky polarization pattern. The results indicate that scattering aerosol mode and absorbing aerosol mode have different effects on sky polarization pattern. Over ocean surface, scattering aerosol tends to decrease the magnitude of sky polarization pattern, while absorbing aerosol tends to increase that. Over land surface, both aerosol modes tend to decrease the magnitude of sky polarization, and scattering aerosol mode is more effectively. The discoveries in our study suggest that to utilize sky polarization pattern information, it is necessary to get detailed aerosol information especially the aerosol mode information.

ARTICLE HISTORY

Received 26 March 2019
Accepted 12 October 2019

1. Introduction

Solar lights reflected by both earth surface (ocean and land) and atmospheric components (molecules and aerosol particles) are partially polarized (Sun and Lukashin 2013). Along with intensity, frequency, and phase, polarization is one of the four major characteristics of electromagnetic waves (Ottaviani, Chowdhary, and Cairns 2019). On the earth, many components are considered to be natural polarizers, such as aerosol, atmospheric molecules, cloud, man-made targets, etc (Sun et al. 2015a; Sun, Videen, and

CONTACT Wei Chen  chenw@cumtb.edu.cn  College of Geoscience and Surveying Engineering, China University of Mining & Technology, Beijing 100083, China

© 2019 The Author(s). Published by Informa UK Limited, trading as Taylor & Francis Group.
This is an Open Access article distributed under the terms of the Creative Commons Attribution-NonCommercial-NoDerivatives License (<http://creativecommons.org/licenses/by-nc-nd/4.0/>), which permits non-commercial re-use, distribution, and reproduction in any medium, provided the original work is properly cited, and is not altered, transformed, or built upon in any way.

Mishchenko 2014). These natural polarizers have different scales of polarization effects. Due to the abundant information polarization provided, it has been applied in various application fields: bionic navigation (Guan et al. 2019), advanced optical material production (Song et al. 2019), and medical applications (Stasinopoulos and Stasinopoulos 2006). Over the past four decades, polarimetric reflective signals have been used in various remote sensing scenarios such as aerosol monitoring (Cheng et al. 2012; Knobelspiesse 2011), cloud property retrieval (Knobelspiesse et al. 2011b), surface characterizing (Waquet et al. 2009; Litvinov et al. 2010), or even navigation (Hamaoui 2017; Ma et al. 2015). However, as human eyes are not sensitive to polarization and the limitation of detectors, the applications of polarimetric signals in remote sensing field is still much less compared with intensity applications (Sun et al. 2018).

To effectively utilize polarimetric reflective signals, a series of air- and space-borne polarized remote sensing sensors have been developed, such as POLarization and Directionality of the Earth's Reflectances (POLDER) developed by Centre National d'Etudes Spatiales of France (Fan et al. 2008; Sun et al. 2015b), Directional Polarimetric Camera (DPC) developed by China (Li et al. 2018), Research Scanning Polarimeter (RSP) as the prototype of Aerosol Polarimetry Sensor (Knobelspiesse et al. 2011a), Ground-based Multi-angle SpectroPolarimetric Imager (Ground MSPI) (Diner et al. 2012). However, compared with massive remote sensing sensors utilizing light intensity (Bilal, Nichol, and Wang 2017; Lee and Kim 2010; Lee, Zhanqing, and Kim 2007; Diner et al. 2005), the number of polarimetric remote sensing sensors is still few.

With these polarimetric remote sensing sensors and vector radiative transfer models, a lot of researches have been done (Xu and Wang 2015; Li et al. 2009). Major applications of polarized remote sensing sensors are aerosol retrieval, mainly for simultaneous retrievals of aerosol optical depth (AOD) and microphysical properties (Wang et al. 2019; Remer et al. 2019; Gao et al. 2019) due to the far more information provided by polarization than intensity only. Some studies focused on the multi-angular properties of cloud to get the optical and microphysical properties of different cloud (Sinclair et al. 2019; Shang et al. 2019; Chen et al. 2019). Through the surface level measurements and modelling, the polarized properties of water surface, or different land surfaces were also investigated (Zhai et al. 2017; Xu et al. 2016; Hou et al. 2018; Sun et al. 2019).

Beside these applications, the sky polarization pattern is one unique application direction of polarimetric remote sensing (Eshelman, Tauc, and Shaw 2019), and is a useful tool in recognizing atmosphere state (Hasekamp, Litvinov, and Butz 2011), navigation application (Chahl and Mizutani 2012), etc. According to Rayleigh scattering theory, a concentric pattern of degree of polarization (DOP) exists in the sky determined by the position of sun. Based on this mechanism, some kinds of creatures could utilize sky polarization pattern to navigate (Chahl and Mizutani 2012; Dacke et al. 2003). Inspired by these smart creatures, scientists have developed more applications of sky polarization pattern. Pomozi, Horvath, and Wehner (2001) revealed that under clear sky conditions, there are also a certain distribution of sky polarization, which could be utilized by insects. Tang et al. (2016) developed a new full-sky polarization imaging sensor, which could get relatively high accuracy of angle of polarization (AOP) under harsh condition. Zhang et al. (2015) found a new way to simulate the sky polarization signal obtained by compound eyes of *Cataglyphis* and validated it through navigation experiments. However, it should be noted that these applications mainly based on Rayleigh scattering theories, with few

considerations of aerosol-loading conditions. For example, to explore the sky polarization pattern, its robust properties are very crucial for bionic application. Zhou et al. (2013) investigated the wave water surface's contribution to the sky polarization pattern, suggesting that the wave's contribution must be considered when simulating sky polarization over ocean. However, in this study only Rayleigh sky condition is considered, the aerosol's influence is neglected. Recognizing the influence of aerosol, Zhao et al. (2018) used AOD to represent pollution conditions, discovering that the sky polarization pattern is not robust, but the distribution pattern of AOP is relatively robust, which coincides with the results demonstrated in Hegedus et al. (2007). Hegedus, Akesson, and Horvath (2007) on the other hand, discovered that direction of polarization is very robust under different sky conditions by full-sky imaging polarimetry. In actual world, both aerosol loading and aerosol microphysical properties (size distribution, refractive index, etc.) will affect sky polarizations, which has not received widespread attention. Therefore, whether different aerosol loading with different aerosol microphysical properties combinations will result different sky polarization pattern changes is still unclear, limiting the applications of sky polarization in such scenarios as bionic navigation.

In this study, the sky polarization pattern variations induced by the changes of aerosol particles have been deeply investigated. Firstly, the vector radiative transfer model and aerosol model are both introduced to illustrate how to calculate the effects of different aerosol particles. Secondly, the single scattering properties of different aerosol particles are calculated to simulate the differences of aerosol particles. Finally, the overall effects of different aerosol particles on sky polarization pattern are discussed to investigate how aerosol changes the sky polarization pattern. Our research is important for applications in polarimetric remote sensing and bionic navigation with sky polarization pattern.

2. Methods

2.1. Theoretical background of polarimetric remote sensing

Light scattered by particles could be fully described by the four Stokes parameters (I , Q , U , and V) as shown in Eq. (1). Under most circumstances, component V could be neglected and degree of linear polarization (DOLP) is the proportion of Q and U in I .

$$\begin{cases} I = E_l E_l^* + E_r E_r^* \\ Q = E_l E_l^* - E_r E_r^* \\ U = E_l E_r^* + E_r E_l^* \\ V = i(E_l E_r^* - E_r E_l^*) \\ \text{DOLP} = \frac{\sqrt{Q^2 + U^2}}{I} \end{cases} \quad (1)$$

Where I is the intensity of light, Q is the radiance component perpendicular (positive) and parallel (negative) to reference plane. U is the intensity component 45° and 135° to the reference plane. Q and U components are called linear polarization components, while V component is called circular component and usually neglected in remote sensing. Subscript l and r represent light vibration parallel and perpendicular to scattering plane. $i = \sqrt{-1}$, E_l (E_r) and E_l^* (E_r^*) represent a pair of complex conjugate of light intensity parallel (perpendicular) to scattering plane. Therefore, in most researches, DOLP is used to represent DOP in remote sensing categories.

In remote sensing, intensity varies when environment changes, such as illumination conditions. Therefore, reflectance, which is the intrinsic characteristic of surface, is used widely. Similarly, polarized reflectance is also defined as the polarized reflected radiance to total reflected radiance in Eq. (2):

$$\begin{cases} R = \frac{\pi I}{E \cos(\theta_s)} \\ R_p = \frac{\pi \sqrt{Q^2 + U^2}}{E \cos(\theta_s)} \end{cases} \quad (2)$$

Where R , and R_p are reflectance and polarized reflectance, respectively. $E \cos(\theta_s)$ is the total irradiance on to the surface. R_p here, similar to DOLP, only considers linear polarization components.

2.2. Aerosol model and radiative transfer model

Light scattering by atmospheric particles (aerosol and molecules) could be described as Eq. (3):

$$\begin{bmatrix} I_v \\ Q_v \\ U_v \\ V_v \end{bmatrix} = F(\Theta) \begin{bmatrix} I_v \\ Q_v \\ U_v \\ V_v \end{bmatrix} = \begin{bmatrix} F_{11} & F_{12} & 0 & 0 \\ F_{21} & F_{22} & 0 & 0 \\ 0 & 0 & F_{33} & F_{34} \\ 0 & 0 & F_{43} & F_{44} \end{bmatrix} \begin{bmatrix} I_0 \\ Q_0 \\ U_0 \\ V_0 \end{bmatrix} \quad (3)$$

Where $F(\Theta)$ is the phase function of particles. Subscript 0 represents incident light and subscript v represents outgoing light. I_0 , Q_0 , U_0 and V_0 are incident light's Stokes components; I_v , Q_v , U_v and V_v are scattering light's Stokes components. For radiative transfer calculation in atmosphere, $F_{12} = F_{21}$, $F_{34} = -F_{43}$. Moreover, the circular polarization components are neglected in remote sensing applications, thus F_{34} , F_{43} and F_{44} are all neglected. For molecule scattering, the phase function could be perfectly described by Rayleigh scattering theories. Despite that, it is non-realistic to only consider Rayleigh conditions because of aerosol particles. Aerosol particles are small particles dispersed in atmosphere with their sizes ranging from 0.01 to 100 μm . Due to the complex sources (natural and anthropogenic) and different sizes, aerosol particles' scattering properties could not be determined easily. That is to say that obtaining an accurate and assured phase function of aerosol is impossible.

Microphysical properties of aerosol (aerosol mode) are the major determinants of aerosol particles' scattering property: such as size distribution functions (lognormal distribution, bi-lognormal distribution, etc., mainly factors characterizing large or small aerosol particles), refractive index (mainly factor determining absorbing characteristics of aerosol), shape factor (spherical and non-spherical), etc. A lot of methods have been developed to calculate scattering properties of aerosol such MIE code (Hu et al. 2019), Discrete-dipole-approximation method (Laczkik 1996), Finite-difference time domain method (Li, Pan, and Zhang 2012), TMatrix method (Farafonov and Ustimov 2015), geometric-optics-integral-equation method (Yang et al. 2007), etc. MIE codes could only process spherical particles whose sizes are comparable with incident light's wavelength, leaving large errors in processing non-spherical large aerosol particles (mainly dust aerosols). To overcome these problems, a TMatrix combined with geometric-optics-integral-equation technique code was utilized to calculate scattering properties with

Table 1. Microphysical characteristics (at 550 nm band) of the aerosol modes used for this study.

Mode	Size	Absorbing characteristic	$r(\mu\text{m})$	σ	n_r	n_i
Mode 1	Coarse mode	Scattering	0.5000	2.99	1.53	0.008
Mode 2	Coarse mode	Absorbing	0.5000	2.99	1.53	0.440
Mode 3	Fine mode	Scattering	0.0118	2.00	1.69	0.008
Mode 4	Fine mode	Absorbing	0.0118	2.00	1.69	0.440

different sizes, shapes and absorbing characteristics (Dubovik et al. 2011, 2006) in this study. The complex phase functions including intensity phase functions and polarized phase functions are all calculated. And these properties could be calculated through the database which could be compiled by Fortran codes (Dubovik et al. 2011). The microphysical parameters of aerosol particles utilized in this study are demonstrated in Table 1. The microphysical parameters of coarse and fine modes refer to the algorithms of MODIS aerosol retrievals (Remer et al. 2005; Vermote et al. 1997). Four types of aerosol modes are included in this study representing coarse mode scattering (dust), coarse mode absorbing (polluted dust), fine mode scattering (small scattering particles), and fine mode absorbing (soot particles). Through TMatrix combined with geometric-optics-integral-equation technique code, the scattering properties including phase function and single scattering albedo are calculated to input to a vector radiative transfer code developed by Dubovik and King (2000) to retrieve aerosol properties of Aerosol Robotic Network (AERONET). It could provide both intensity and linear polarization reflective signals for plane parallel atmosphere conditions. The molecule scattering is already coupled into the radiative transfer code, while the scattering properties of aerosols need to be input into with specific format. In this study, the profile of aerosol vertical distribution is assumed to be exponential distribution with scale height of 2km while the molecule vertical distribution is also assumed to be exponential distribution.

2.3. Surface reflection

Surface reflection, including intensity reflectance and polarized reflectance, is another important factor affecting polarized signal obtained by space-borne sensors. As sky polarization pattern is mainly obtained through downward polarized signals, the reflected signal may contribute less considering the large contributions from direct and diffuse solar light. In this study, we consider two kinds of underlying surfaces: ocean and vegetated land surface as sensitivity study.

For ocean surface, reflectance of ocean surface could be described as the sum of three independent components as Eq. (4):

$$\rho_{os} = \rho_{wc} + (1 - W)\rho_{gl} + (1 - \rho_{wc}) \times \rho_{sw} \quad (4)$$

Where ρ_{os} is the reflectance of ocean surface, ρ_{wc} is the reflectance due to whitecaps of ocean, ρ_{gl} is the specular reflectance of ocean surface, ρ_{sw} is the volume scattering of ocean body. W is the relatively area covered with whitecaps and could be determined by wind speed and wind directions. For these three parts of reflectance, it is assumed the ρ_{gl} is the major cause of polarized reflectance of ocean surface. For wave ocean surface, the distribution of facets (small specular ocean surface) is considered to derive the polarized reflectance of ocean surface as suggested in Cox and Munk (1954) and Zhou et al. (2013).

For land surface, Rahman-Pinty-Verstraete (RPV) model was adopted to simulate the surface bidirectional reflectance with three parameters as Eq. (5):

$$\rho_s = \rho_0 \frac{\cos^{k-1}\theta_s \cos^{k-1}\theta_v}{(\cos\theta_s + \cos\theta_v)^{1-k}} F(g) [1 + R(G)] \tag{5}$$

Where ρ_s is the reflectance from a view direction, θ_s and θ_v are solar zenith angle and view zenith angle, respectively. ρ_0 is the arbitrary parameter characterizing the reflectance of the surface cover, k is the structural parameter, $R(G)$ is the parameter to describe hotspot effect. $F(g)$ and $R(G)$ could be described as Eq. (6):

$$F(g) = \frac{1 - \Theta^2}{[1 + \Theta^2 - 2\Theta(\pi - g)]^{1.5}}$$

$$\cos g = \cos\theta_s \cos\theta_v + \sin\theta_s \sin\theta_v \cos(\phi_s - \phi_v)$$

$$R(G) = \frac{1 - \rho_0}{1 + G}$$

$$G = [\tan^2\theta_s + \tan^2\theta_v - 2\tan\theta_s \tan\theta_v \cos(\phi_s - \phi_v)]^{0.5} \tag{6}$$

Where Θ is the asymmetry factor, ϕ_s and ϕ_v are solar azimuth angle and view azimuth angle, respectively. As this study mainly focuses on downward sky light, the contribution of surface reflectance’s re-backscattering may be very few. Therefore, we only considered a simple dense vegetation case, which is widely used in aerosol retrieval. As suggested in Sun et al. (2017), the RPV model of vegetation surface could be parameterized as Table 2:

For polarized reflectance of vegetation surface, the Maignan model with only one free parameter was adopted as shown in Eq. (7). The Maignan model was validated as simple, high accuracy compared with other models and surface measurements (Yang, Zhao, and Chen 2017).

$$R_p = \frac{C \times \exp(-\tan\theta_i) \times \exp(-NDVI) \times F_p(\gamma, N)}{4(\mu_s + \mu_v)}$$

$$F_p(\gamma, N) = \frac{1}{2} \left[\left(\frac{N \mu_t - \mu_i}{N \mu_t + \mu_i} \right)^2 - \left(\frac{N \mu_i - \mu_t}{N \mu_i + \mu_t} \right)^2 \right]$$

$$\mu_i = \cos\theta_i, \mu_t = \cos\theta_t$$

$$\sin\theta_i = N \sin\theta_t, \theta_i = (\pi - \gamma)/2$$

$$\cos\gamma = -\cos\theta_s \cos\theta_v - \sin\theta_s \sin\theta_v \cos\varphi. \tag{7}$$

Table 2. RPV model parameters of vegetation surface.

Wavelength	ρ_0	g	k
550 nm	0.052	0.2232	1.1094

Where C is the free parameter, $F_p(\gamma, N)$ is the Fresnel equation; N is the refractive index of surface, usually defined as 1.5 for land surface and 1.33 for water; θ_i and θ_t are angles of specular reflection and refraction; γ is the scattering angle; μ_i and μ_t are the cosine of solar zenith angle and view zenith angle. φ is the relative azimuth angle between solar azimuth angle and view azimuth angle.

In the vector radiative transfer model adopted in this study, the ocean surface and ocean polarized reflectance could be directly computed within the code by setting wind speed and refractive index. For land surface, reflectance could be obtained inside the code by defining the three parameters in RPV model, while for polarized reflectance, a new subroutine is written to overwrite the original Nadal–Bréon model provided by the original code considering the accuracy of these models (Maignan et al. 2009). In this study, a vegetation underlying surface is assumed with coefficient 'C' to be set as 3.885 according to previous model comparisons (Yang, Zhao, and Chen 2017).

3. Results and discussion

3.1. Single scattering properties of different aerosol models

The single scattering properties of different aerosol modes (mainly considering the size, absorbing properties) may be very different. Firstly, the absorbing characteristics' effects on the single scattering properties are analysed. The phase function parameters (F_{11} , F_{12} , F_{22} , and F_{33}) in 550 nm band are demonstrated as shown in Figure 1. For both coarse mode and fine mode aerosol mode, 10 different absorbing levels are demonstrated by assigning these aerosol modes with different imaginary part values in refractive index. It could be found that the absorbing characteristics have significant influences on the single scattering properties of aerosol. For F_{11} , the absorbing characteristics mainly affect the backscattering directions (scattering angle larger than 90°). For F_{12} and F_{22} , the major phase function parameters characterizing polarization properties of scattering light, it could be found that the absorbing aerosol mode has larger values than scattering aerosol mode, suggesting that absorbing characteristics will have large influence on the polarization characteristics of scattering light. For F_{33} , the differences between scattering and absorbing aerosol modes are also obvious.

Figure 2 phase function parameters of coarse mode and fine mode aerosols in 550 nm band with different absorbing characteristics as shown in Table 1. (a) F_{11} ; (b) F_{12} ; (c) F_{22} ; (d) F_{33} .

3.2. Sky polarization pattern upon ocean surface

The polarization states of a skylight could be useful in navigation of a lot of insects as well as human beings by analyzing the sky polarization pattern in the sky. It is assumed that there is a relatively robust sky polarization pattern mainly determined by the position of sun and influenced by Rayleigh scattering and aerosol disturbances. Most current research mainly considered Rayleigh scattering conditions (Zhou et al. 2013), or different AOD (Zhao et al. 2018). However, it should be noted that both molecules and aerosol particles could strongly polarize incident light in different directions, which may enhance or weaken the overall polarization of outgoing light. As a result, it is not suitable to obtain sky polarization pattern considering merely Rayleigh scattering while neglecting aerosol

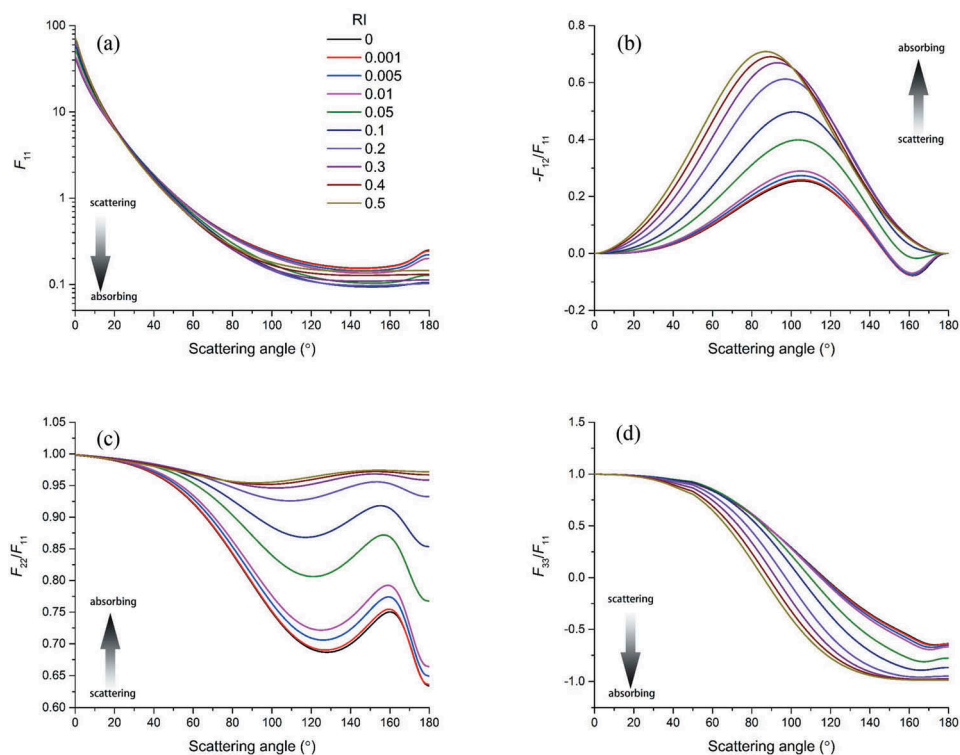


Figure 1. Phase function parameters of coarse mode aerosols in 550 nm band with different absorbing characteristics (RI is the imaginary part of refractive index of aerosol; the larger RI is, the more absorbing the aerosol). (a) F_{11} ; (b) F_{12} ; (c) F_{22} ; (d) F_{33} .

effects, especially aerosol mode information. With the phase functions of four different aerosol modes: coarse scattering, coarse absorbing, fine scattering, and fine absorbing, the sky polarization patterns of different aerosol loadings and different aerosol modes are presented here. In this section, the ocean surface conditions are presented.

Figure 3 demonstrates the sky polarization pattern variations when AOD increase from 0 to 0.5 with different aerosol modes. In Figure 3, we only simulated atmosphere conditions with only one aerosol components. Overall, under different aerosol loading conditions, the sky polarization is similar: the direction of solar incidence has the least DOP nearly reaching 0, suggesting that the direct solar light is nearly neutral; centring the solar position, DOP gradually increases outward with the largest DOP occurring around the specular direction. These results suggest that Rayleigh scattering has determined the basic pattern of sky polarization, while variations of aerosol loading may change the magnitude of this pattern. When coarse scattering aerosol loading increases, the magnitude of sky polarization has decreased sharply from a maximum DOP of 0.7 to 0.5. For coarse absorbing aerosol conditions, when AOD increases, the sky polarization does not decrease but has slightly increase, which is different from coarse scattering aerosol conditions. This result is very interesting as it reveals that the sky polarization is not sensitive to this kind of aerosol (coarse absorbing). For fine scattering and fine absorbing aerosol conditions, the cases are somehow different. When fine scattering aerosol loading increases, sky polarization pattern

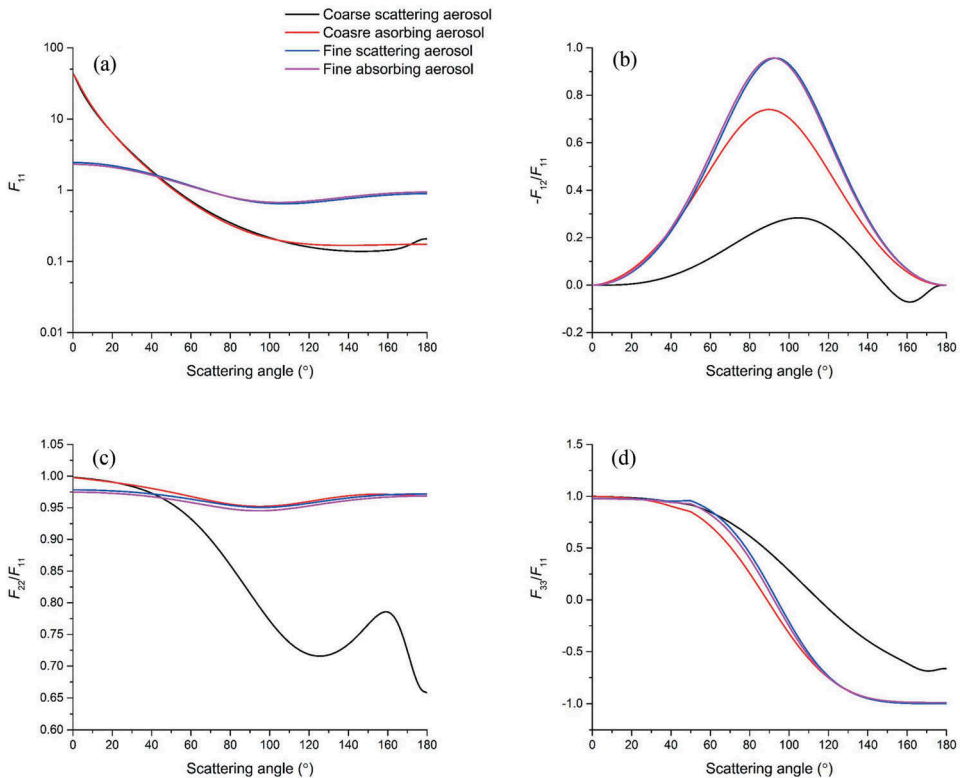


Figure 2. Demonstrates the influences of aerosol sizes and absorbing characteristics in 550 nm band. The parameters of four different aerosol modes are illustrated in Table 1. For F_{11} , the differences of size parameters (median radius and standard deviation) dominate. There are huge differences between coarse mode and fine mode aerosols. While for F_{12} , F_{22} and F_{33} , the absorbing characteristics and size parameters both contribute to the differences. These results all suggested that, the aerosol mode may play an important role in the polarized scattering characteristics of atmosphere.

decreases from a maximum DOP of 0.7 to 0.4. While fine absorbing aerosol loading increases, the sky polarization pattern increases more obvious than that of coarse absorbing aerosol conditions.

The results revealed by Figure 3 suggest that aerosol mode has significant influence on the magnitude of sky polarization but will not change the basic pattern. Even when the AOD is same, different aerosol modes will result in different sky polarization pattern strength. In actual aerosol retrieval, it is impossible that only one aerosol mode exists. Most researches have assumed that one coarse mode and one fine mode in aerosol exist. Therefore, whether the combination of different will offset the sky polarization pattern? Four kinds of combinations are demonstrated in this study as shown in Figure 4: coarse scattering + fine scattering, coarse scattering + fine absorbing, coarse absorbing + fine scattering, and coarse absorbing + fine absorbing.

As shown in Figure 4, when both coarse scattering and fine scattering aerosol exist, the sky polarization pattern trends to decrease when total AOD increases. When coarse scattering and fine absorbing aerosols combined, the coarse scattering aerosol tends to decrease DOP while fine absorbing aerosol tends to increase the DOP. The overall effect of

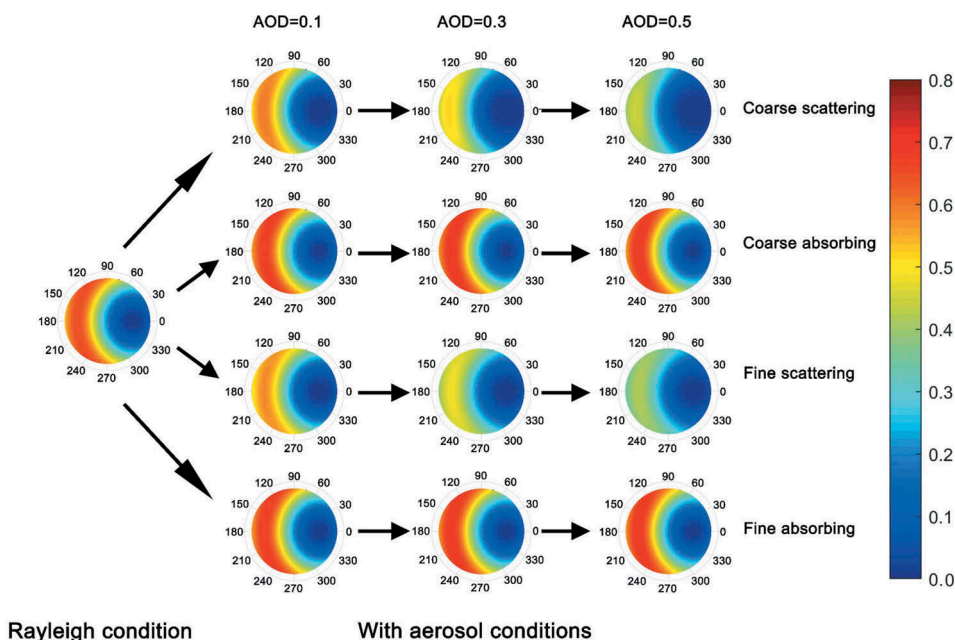


Figure 3. Sky polarization pattern over ocean surface with different aerosol loading when only one aerosol component exists (the solar zenith is 40° , solar azimuth is 0° , the first row is the case of coarse scattering aerosol condition, the second row is coarse absorbing aerosol condition, the third row is fine scattering aerosol condition, and the fourth row is the fine absorbing condition. The columns represent different AOD conditions. The colour bar represents DOP which is unit free.).

this combination is a slightly decrease of sky polarization pattern magnitude. Similar trends could also be observed for the combination of coarse absorbing and fine scattering aerosols, whose decreasing trend is slower. The combination of two absorbing aerosol will slightly increase the sky polarization pattern magnitude. Additionally, it could be found that scattering aerosol tends to decrease the sky polarization pattern magnitude while absorbing aerosol tends to increase the sky polarization pattern. Fine scattering aerosol is more effective in decreasing sky polarization, while coarse absorbing aerosol is more effective in increasing sky polarization.

3.3. Sky polarization pattern upon land surface

Ocean surface is relatively simple as the ocean surface's reflectance is relatively low at visible and near-infrared bands, making it contribute little to the sky polarization pattern. However, the heterogeneity and non-lambert properties of land surface make the contribution of land surface non-negligible. With RPV model and Maignan model, the BRDF and BPDF properties of land surface (vegetation surface in this study) are calculated. The sky polarization patterns under different aerosol loadings and aerosol models same as Section 3.2 are presented as shown in Figures 5 and 6. Figure 5 demonstrates the sky polarization pattern variations over land surface with one aerosol mode same as Figure 3. Firstly, the basic pattern of sky polarization is similar. The lowest

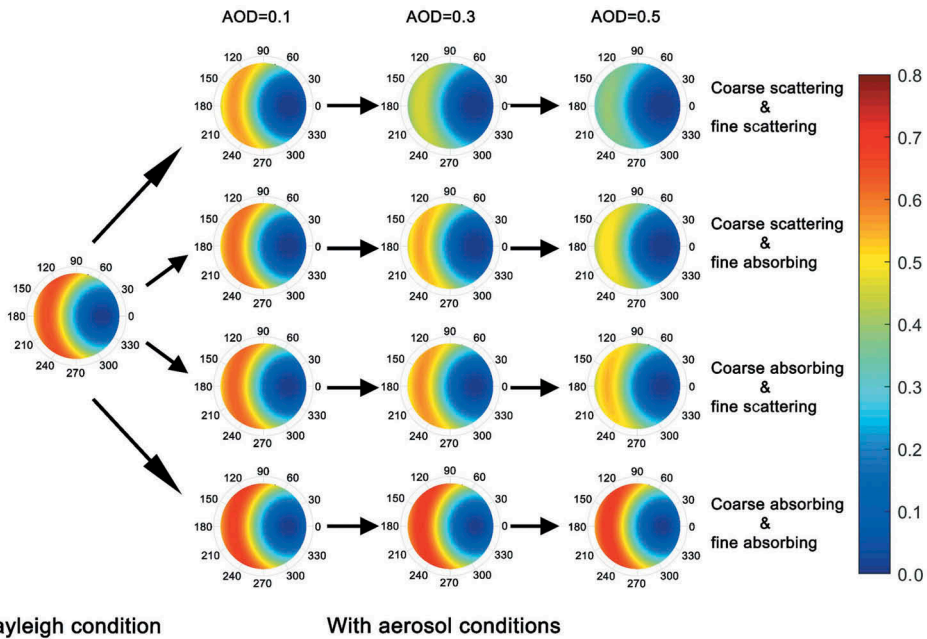


Figure 4. Sky polarization pattern over ocean surface with different aerosol loading when only two component exist (the solar zenith is 40° , solar azimuth is 0° , the first row is the case of coarse scattering + fine scattering aerosol condition, the second row is coarse scattering + fine absorbing aerosol condition, the third row is coarse absorbing + fine scattering aerosol condition, and the forth row is coarse absorbing + fine absorbing aerosol condition. The columns represent different AOD conditions. The colour bar represents DOP which is unit free.).

DOP occurs around the solar incident direction. Secondly, the magnitudes of sky polarization pattern over land are systematically larger (10–20%) than those over ocean surface. For Rayleigh sky, the largest DOP over land could be higher than 0.8 compared with only 0.7 over ocean. For scattering aerosol conditions (coarse mode and fine mode), the increase of AOD will greatly decrease the magnitude of sky polarization pattern, which is also similar to those cases over ocean surface. While for absorbing aerosol conditions, the cases are different from those over ocean surface. The increase absorbing AOD also makes the sky polarization pattern decrease, but with a much lower speed than scattering AOD does.

Figure 6 demonstrates the sky polarization pattern variations over land surface with aerosol combinations same as Figure 4. The combination of coarse scattering and fine scattering aerosol also makes the sky polarization decrease greatly from a maximum value of over 0.8 to 0.5. When one absorbing aerosol is included, the decrease trend is much slower. Furthermore, the two absorbing aerosol combination only makes the sky polarization decrease a little. These results suggest that, over land surface, the coupling between atmosphere and land surface is complicated. The sky polarization is determined by not only Rayleigh scattering of atmospheric molecules, aerosol particles, but also surface contribution, making the variation trends of sky polarization complicated and unpredictable whether any information mentioned above is lacking. However, although

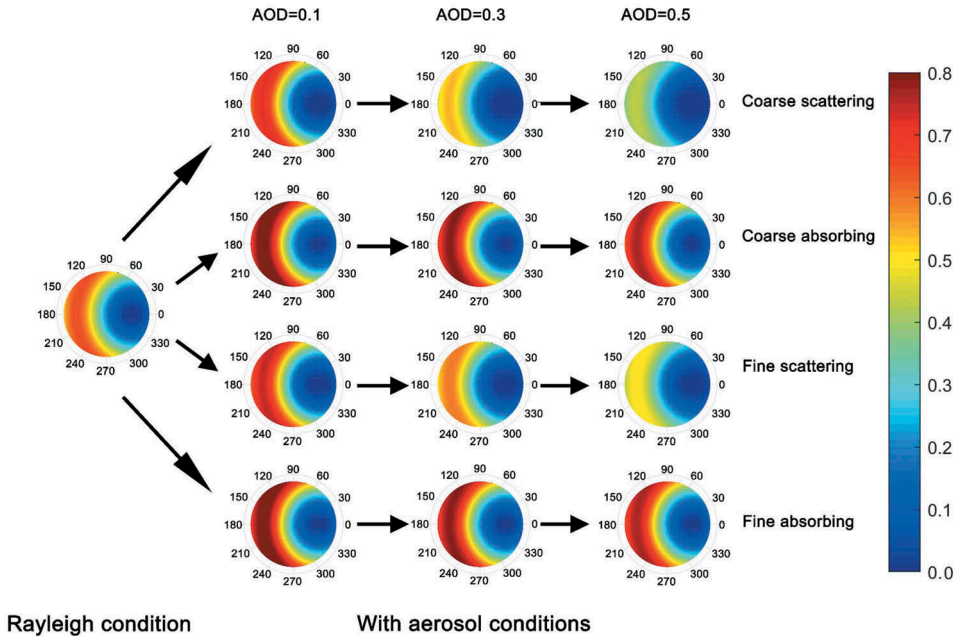


Figure 5. Sky polarization pattern over land surface with different aerosol loading when only one aerosol component exists (the solar zenith is 40° , solar azimuth is 0° , the first row is the case of coarse scattering aerosol condition, the second row is coarse absorbing aerosol condition, the third row is fine scattering aerosol condition, and the fourth row is the fine absorbing condition. The columns represent different AOD conditions. The colour bar represents DOP which is unit free.)

the variation trends are sophisticated, the morphology of sky polarization pattern is relatively stable, centring the solar position and increasing outward.

3.4. Implications and limitations and future work

All previous researches have mentioned that the sky polarization pattern is influenced by atmosphere conditions. However, most researches have no specific or only limited description of atmospheric conditions. AOD, aerosol models, surface reflectance, as well as cloud conditions are all possible influence factors. Only considering AOD conditions is really not sufficient to evaluate the sky polarization pattern variation trends. Our researches here, by combining AOD, aerosol mode information, and underlying surface conditions, find that the sky polarization pattern variation trends are the results of complex interactions of these factors. It is not realistic to predict the sky polarization pattern strength whether lacking any information mentioned above. Therefore, when applying sky polarization, it should be cautious when aerosol mode information is lacking. Despite that, the basic pattern (shape) of sky polarization is relatively robust.

There are several limitations to this study. Firstly, only four lognormal distribution aerosol modes are selected in this study. These aerosol modes are not enough to describe the real atmospheric conditions. Secondly, we only perform the results in 550 nm band. The scattering and polarization states at other bands, such as blue band (440 nm) and

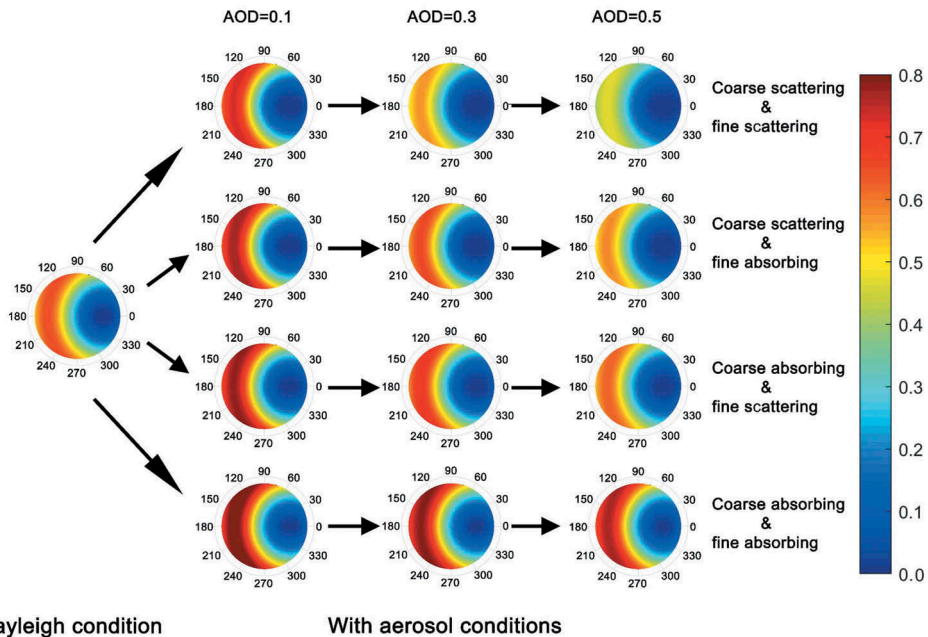


Figure 6. Sky polarization pattern over land surface with different aerosol loading when only two component exist (the solar zenith is 40° , solar azimuth is 0° , the first row is the case of coarse scattering + fine scattering aerosol condition, the second row is coarse scattering + fine absorbing aerosol condition, the third row is coarse absorbing + fine scattering aerosol condition, and the forth row is coarse absorbing + fine absorbing aerosol condition. The columns represent different AOD conditions. The colour bar represents DOP which is unit free.).

infrared band (860 nm) may be different due to different strength of atmospheric scattering and absorbing, although the results may be similar. Thirdly, the land surface reflectance contribution is obtained through empirical BRDF model, which may be different from the complex land surface conditions. Finally, the cloud condition is not considered in this study due to the limitation of current vector radiative transfer model.

In the future, to further investigate aerosol's influence on sky polarization pattern, more aerosol mode information will be considered by reference the aerosol retrieval algorithm of MODIS (Li et al. 2007), MISR (Diner et al. 2005), POLDER (Hasekamp, Litvinov, and Butz 2011) to validate our results. Furthermore, different BRDF and BPDF will be evaluated to make our result robust and convincing. Finally, more characteristic bands will be considered to explore which band will get the more robust sky polarization pattern.

4. Conclusions

Sky polarization pattern is caused by the interaction between incident solar light and atmospheric components (aerosol and molecules). Both aerosol particles and molecules could polarize the incident neutral light. A lot of researches focusing on the application of sky polarization pattern mainly assume a Rayleigh sky which is not accurate enough to describe the real sky situations, restricting the further application of sky polarization pattern. As both aerosol particles and molecules contribute to the generation of sky

polarization, the simulation and application of sky polarization pattern should consider aerosol situations. However, current research, which take aerosol into account only consider AOD information, neglecting the intrinsic microphysical properties of aerosol (size distribution, refractive index, etc.).

In this study, both AOD and aerosol mode information are considered in the generation of sky polarization pattern. Our researches reveal that the basic pattern of sky polarization is generated through Rayleigh scattering, and the increase of different aerosol loading will not change the basic pattern but change the magnitude. Additionally, different aerosol modes' effects on sky polarization pattern over different underlying surfaces are different. Over ocean surface, where the reflectance is relatively low, scattering aerosol tends to weaken sky polarization pattern, while absorbing aerosol tends to slightly strengthen it. Furthermore, coarse mode scattering aerosol is more effective in weaken sky polarization pattern than fine mode scattering aerosol. Over land surface, where the reflectance is relatively high, both scattering and absorbing aerosols tend to weaken the sky polarization pattern. The scattering aerosol is more effective than absorbing aerosol.

The results in our study suggest that aerosol's influences on sky polarization pattern are sophisticated. The increase of AOD does not absolutely mean a decrease of sky polarization. Under some polluted situation with strong absorbing aerosol loading, the sky polarization will keep stable or even increase. Therefore, to utilize sky polarization pattern for bionic application such as navigation, it should be cautious to be aware of the effects of both AOD and aerosol modes.

Disclosure statement

No potential conflict of interest was reported by the authors.

Funding

This work was supported by the National Natural Science Foundation of China [41701391, 41801227,61841101]; National Natural Science Foundation of China; Beijing Natural Science Foundation [8192037]; Fundamental Research Funds for the Central Universities [2014QD02].

ORCID

Wei Chen  <http://orcid.org/0000-0002-2585-9984>
Hao Sun  <http://orcid.org/0000-0001-5705-9749>
Hengqian Zhao  <http://orcid.org/0000-0003-0776-142X>
Jouni Peltoniemi  <http://orcid.org/0000-0002-4701-128X>

References

- Bilal, M., J. E. Nichol, and L. C. Wang. 2017. "New Customized Methods for Improvement of the MODIS C6 Dark Target and Deep Blue Merged Aerosol Product." *Remote Sensing of Environment* 197: 115–124. doi:10.1016/j.rse.2017.05.028.
- Chahl, J., and A. Mizutani. 2012. "Biomimetic Attitude and Orientation Sensors." *IEEE Sensors Journal* 12 (2): 289–297. doi:10.1109/jsen.2010.2078806.

- Chen, C.-Y., P. K. King, L. Zhi-Yun, L. M. Fissel, and R. R. Mazzei. 2019. "A New Method to Trace Three-dimensional Magnetic Field Structure within Molecular Clouds Using Dust Polarization." *Monthly Notices of the Royal Astronomical Society* 485 (3): 3499–3513. doi:10.1093/mnras/stz618.
- Cheng, T., X. Gu, D. Xie, Z. Li, T. Yu, and H. Chen. 2012. "Aerosol Optical Depth and Fine-mode Fraction Retrieval over East Asia Using Multi-angular Total and Polarized Remote Sensing." *Atmospheric Measurement Techniques* 5 (3): 501–516. doi:10.5194/amt-5-501-2012.
- Cox, C., and W. Munk. 1954. "Measurement of the Roughness of the Sea Surface from Photographs of the Sun's Glitter." *Journal of the Optical Society of America* 44 (11): 838–850. doi:10.1364/josa.44.000838.
- Dacke, M., D. E. Nilsson, C. H. Scholtz, M. Byrne, and E. J. Warrant. 2003. "Insect Orientation to Polarized Moonlight." *Nature* 424 (6944): 33. doi:10.1038/424033a.
- Diner, D., F. Xu, J. Martonchik, B. Rheingans, S. Geier, V. Jovanovic, A. Davis, R. Chipman, and S. McClain. 2012. "Exploration of a Polarized Surface Bidirectional Reflectance Model Using the Ground-Based Multiangle SpectroPolarimetric Imager." *Atmosphere* 3 (4): 591. doi:10.3390/atmos3040591.
- Diner, D. J., J. V. Martonchik, R. A. Kahn, B. Pinty, N. Gobron, D. L. Nelson, and B. N. Holben. 2005. "Using Angular and Spectral Shape Similarity Constraints to Improve MISR Aerosol and Surface Retrievals over Land." *Remote Sensing of Environment* 94 (2): 155–171. doi:10.1016/j.res.2004.09.009.
- Dubovik, O., M. Herman, A. Holdak, T. Lapyonok, D. Tanr, J. L. Deuz', F. Ducos, A. Sinyuk, and A. Lopatin. 2011. "Statistically Optimized Inversion Algorithm for Enhanced Retrieval of Aerosol Properties from Spectral Multi-angle Polarimetric Satellite Observations." *Atmospheric Measurement Techniques* 4: 975–1018. doi:10.5194/amt-4-975-2011.
- Dubovik, O., and M. D. King. 2000. "A Flexible Inversion Algorithm for Retrieval of Aerosol Optical Properties from Sun and Sky Radiance Measurements." *Journal of Geophysical Research* 105 (D16): 20673–20696. doi:10.1029/2000JD900282.
- Dubovik, O., A. Sinyuk, T. Lapyonok, B. N. Holben, M. Mishchenko, P. Yang, T. F. Eck, et al. 2006. "Application of Spheroid Models to Account for Aerosol Particle Nonsphericity in Remote Sensing of Desert Dust." *Journal of Geophysical Research* 111 (D11): D11208. doi:10.1029/2005jd006619.
- Eshelman, L. M., M. J. Tauc, and J. A. Shaw. 2019. "All-sky Polarization Imaging of Cloud Thermodynamic Phase." *Optics Express* 27 (3): 3528–3541. doi:10.1364/oe.27.003528.
- Fan, X. H., P. Goloub, J. L. Deuze, H. B. Chen, W. X. Zhang, D. Tanre, and Z. Q. Li. 2008. "Evaluation of PARASOL Aerosol Retrieval over North East Asia." *Remote Sensing of Environment* 112 (3): 697–707. doi:10.1016/j.rse.2007.06.010.
- Farafonov, V. G., and V. I. Ustimov. 2015. "Properties of the T Matrix in the Rayleigh Approximation." *Optics and Spectroscopy* 119 (6): 1022–1033. doi:10.1134/s0030400x15120103.
- Gao, M., B. A. Peng-Wang Zhai, Y. H. Franz, P. Kirk Knobelspiesse, J. Werdell, A. Ibrahim, B. Cairns, and A. Chase. 2019. "Inversion of Multiangular Polarimetric Measurements over Open and Coastal Ocean Waters: A Joint Retrieval Algorithm for Aerosol and Water-leaving Radiance Properties." *Atmospheric Measurement Techniques* 12 (7): 3921–3941. doi:10.5194/amt-12-3921-2019.
- Guan, L., S. Liu, J. Chu, R. Zhang, Y. Chen, L. Shiqi, L. Zhai, L. Yinnan, and H. Xie. 2019. "A Novel Algorithm for Estimating the Relative Rotation Angle of Solar Azimuth through Single-pixel Rings from Polar Coordinate Transformation for Imaging Polarization Navigation Sensors." *Optik* 178: 868–878. doi:10.1016/j.ijleo.2018.10.080.
- Hamaoui, M. 2017. "Polarized Skylight Navigation." *Applied Optics* 56 (3): B37–B46. doi:10.1364/ao.56.000b37.
- Hasekamp, O. P., P. Litvinov, and A. Butz. 2011. "Aerosol Properties over the Ocean from PARASOL Multiangle Photopolarimetric Measurements." *Journal of Geophysical Research* 116. doi:10.1029/2010jd015469.
- Hegedus, R., S. Akesson, and G. Horvath. 2007. "Polarization Patterns of Thick Clouds: Overcast Skies Have Distribution of the Angle of Polarization Similar to that of Clear Skies." *Journal of the Optical Society of America a-Optics Image Science and Vision* 24 (8): 2347–2356. doi:10.1364/josaa.24.002347.
- Hegedus, R., A. Barta, B. Bernath, V. B. Meyer-Rochow, and G. Horvath. 2007. "Imaging Polarimetry of Forest Canopies: How the Azimuth Direction of the Sun, Occluded by Vegetation, Can Be

- Assessed from the Polarization Pattern of the Sunlit Foliage." *Applied Optics* 46 (23): 6019–6032. doi:10.1364/ao.46.006019.
- Hou, W., L. Zhengqiang, J. Wang, X. Xiaoguang, P. Goloub, and L. Qie. 2018. "Improving Remote Sensing of Aerosol Microphysical Properties by Near-Infrared Polarimetric Measurements over Vegetated Land: Information Content Analysis." *Journal of Geophysical Research-Atmospheres* 123 (4): 2215–2243. doi:10.1002/2017jd027388.
- Hu, S., X. Chidong, J. Yufeng, and H. Huanling. 2019. "Aerosol Microphysical Parameters' Vertical Profiles Measured by a Dual Raman-Mie Lidar during 2007–2013 at Hefei, China." *Applied Optics* 58 (6): 1537–1546. doi:10.1364/ao.58.001537.
- Knobelspiesse, K., B. Cairns, M. Ottaviani, R. Ferrare, J. Hair, C. Hostetler, M. Obland, et al. 2011a. "Combined Retrievals of Boreal Forest Fire Aerosol Properties with a Polarimeter and Lidar." *Atmospheric Chemistry and Physics* 11 (14): 7045–7067. doi:10.5194/acp-11-7045-2011.
- Knobelspiesse, K., B. Cairns, J. Redemann, R. W. Bergstrom, and A. Stohl. 2011b. "Simultaneous Retrieval of Aerosol and Cloud Properties during the MILAGRO Field Campaign." *Atmospheric Chemistry and Physics* 11 (13): 6245–6263. doi:10.5194/acp-11-6245-2011.
- Knobelspiesse, K. D. 2011. "Atmospheric aerosol optical property retrieval with scanning polarimeters." Columbia University.
- Laczik, Z. 1996. "Discrete-dipole-approximation-based Light-scattering Calculations for Particles with a Real Refractive Index Smaller than Unity." *Applied Optics* 35 (19): 3736–3745. doi:10.1364/ao.35.003736.
- Lee, K. H., and Y. J. Kim. 2010. "Satellite Remote Sensing of Asian Aerosols: A Case Study of Clean, Polluted, and Asian Dust Storm Days." *Atmospheric Measurement Techniques* 3 (6): 1771–1784. doi:10.5194/amt-3-1771-2010.
- Lee, K. H., L. Zhanqing, and Y. J. Kim. 2007. "SWIR/VIS Reflectance Ratio over Korea for Aerosol Retrieval." *Korean Journal of Remote Sensing* 23 (1): 1–5.
- Li, H., S. Pan, and Y. Zhang. 2012. "Finite-difference Time Domain Method for Light Scattering by Nano Coil Structure in Three-dimensional Space." In *6th International Symposium on Advanced Optical Manufacturing and Testing Technologies: Design, Manufacturing, and Testing of Smart Structures, Micro- and Nano- Optical Devices, and Systems*, edited by T. Ye, X. Luo, S. Hu, X. Bao, and Y. Li. Xiamen, China.
- Li, Z., P. Goloub, O. Dubovik, L. Blarel, W. Zhang, T. Podvin, A. Sinyuk, et al. 2009. "Improvements for Ground-based Remote Sensing of Atmospheric Aerosol Properties by Additional Polarimetric Measurements." *Journal of Quantitative Spectroscopy & Radiative Transfer* 110 (17): 1954–1961. doi:10.1016/j.jqsrt.2009.04.009.
- Li, Z. Q., W. Z. Hou, J. Hong, F. X. Zheng, D. G. Luo, J. Wang, X. F. Gu, and Y. L. Qiao. 2018. "Directional Polarimetric Camera (DPC): Monitoring Aerosol Spectral Optical Properties over Land from Satellite Observation." *Journal of Quantitative Spectroscopy & Radiative Transfer* 218: 21–37. doi:10.1016/j.jqsrt.2018.07.003.
- Li, Z. Q., F. Niu, K. H. Lee, J. Y. Xin, W. M. Hao, B. Nordgren, Y. S. Wang, and P. C. Wang. 2007. "Validation and Understanding of Moderate Resolution Imaging Spectroradiometer Aerosol Products (C5) Using Ground-based Measurements from the Handheld Sun Photometer Network in China." *Journal of Geophysical Research* 112 (D22): D22s09. doi:10.1029/2007jd008479.
- Litvinov, P., O. Hasekamp, B. Cairns, and M. Mishchenko. 2010. "Reflection Models for Soil and Vegetation Surfaces from Multiple-viewing Angle Photopolarimetric Measurements." *Journal of Quantitative Spectroscopy & Radiative Transfer* 111 (4): 529–539. doi:10.1016/j.jqsrt.2009.11.001.
- Ma, T., X. P. Hu, L. L. Zhang, J. X. Lian, X. F. He, Y. J. Wang, and Z. W. Xian. 2015. "An Evaluation of Skylight Polarization Patterns for Navigation." *Sensors* 15 (3): 5895–5913. doi:10.3390/s150305895.
- Maignan, F., F. M. Bréon, E. Fedele, and M. Bouvier. 2009. "Polarized Reflectances of Natural Surfaces: Spaceborne Measurements and Analytical Modeling." *Remote Sensing of Environment* 113 (12): 2642–2650. doi:10.1016/j.rse.2009.07.022.
- Ottaviani, M., J. Chowdhary, and B. Cairns. 2019. "Remote Sensing of the Ocean Surface Refractive Index via Short-wave Infrared Polarimetry." *Remote Sensing of Environment* 221: 14–23. doi:10.1016/j.rse.2018.10.016.

- Pomozi, I., G. Horvath, and R. Wehner. 2001. "How the Clear-sky Angle of Polarization Pattern Continues Underneath Clouds: Full-sky Measurements and Implications for Animal Orientation." *Journal of Experimental Biology* 204 (17): 2933–2942.
- Remer, L. A., Y. J. Kaufman, D. Tanre, S. Mattoo, D. A. Chu, J. V. Martins, -R.-R. Li, et al. 2005. "The MODIS Aerosol Algorithm, Products, and Validation." *Journal of the Atmospheric Sciences* 62 (4): 947–973. doi:10.1175/jas3385.1.
- Remer, L. A., K. Knobelspiesse, P.-W. Zhai, X. Feng, O. V. Kalashnikova, J. Chowdhary, O. Hasekamp, et al. 2019. "Retrieving Aerosol Characteristics from the PACE Mission, Part 2: Multi-Angle and Polarimetry." *Frontiers in Environmental Science* 7. doi:10.3389/fenvs.2019.00094.
- Shang, H., H. Letu, F.-M. Breon, J. Riedi, M. Run, T. Y. Ziming Wang, Z. W. Nakajima, and L. Chen. 2019. "An Improved Algorithm of Cloud Droplet Size Distribution from POLDER Polarized Measurements." *Remote Sensing of Environment* 228: 61–74. doi:10.1016/j.rse.2019.04.013.
- Sinclair, K., B. van Diedenhoven, B. Cairns, M. Alexandrov, R. Moore, E. Crosbie, and L. Ziemba. 2019. "Polarimetric Retrievals of Cloud Droplet Number Concentrations." *Remote Sensing of Environment* 228: 227–240. doi:10.1016/j.rse.2019.04.008.
- Song, B., G. Honggang, M. Fang, X. Chen, H. Jiang, R. Wang, T. Zhai, H. Yen-Teng, and S. Liu. 2019. "Layer-Dependent Dielectric Function of Wafer-Scale 2D MoS₂." *Advanced Optical Materials* 7: 2. doi:10.1002/adom.201801250.
- Stasinopoulos, D., and I. Stasinopoulos. 2006. "Comparison of Effects of Cyriax Physiotherapy, a Supervised Exercise Programme and Polarized Polychromatic Non-coherent Light (Biopton light) for the Treatment of Lateral Epicondylitis." *Clinical Rehabilitation* 20 (1): 12–23. doi:10.1191/0269215506cr9210a.
- Sun, W., R. R. Baize, G. Videen, Y. Hu, and Q. Fu. 2015a. "A Method to Retrieve Super-thin Cloud Optical Depth over Ocean Background with Polarized Sunlight." *Atmospheric Chemistry and Physics* 15 (20): 11909–11918. doi:10.5194/acp-15-11909-2015.
- Sun, W., and C. Lukashin. 2013. "Modeling Polarized Solar Radiation from the Ocean-atmosphere System for CLARREO Inter-calibration Applications." *Atmospheric Chemistry and Physics* 13 (20): 10303–10324. doi:10.5194/acp-13-10303-2013.
- Sun, W., C. Lukashin, R. R. Baize, and D. Goldin. 2015b. "Modeling Polarized Solar Radiation for CLARREO Inter-calibration Applications: Validation with PARASOL Data." *Journal of Quantitative Spectroscopy & Radiative Transfer* 150: 121–133. doi:10.1016/j.jqsrt.2014.05.013.
- Sun, W., G. Videen, and M. I. Mishchenko. 2014. "Detecting Super- Thin Clouds with Polarized Sunlight." *Geophysical Research Letters* 41 (2): 688–693. doi:10.1002/2013gl058840.
- Sun, W., B. A. Wielicki, R. R. Baize, C. Lukashin, H. Yongxiang, E. Zubko, G. Videen, S. S. Kim, and Y.-J. Choi. 2019. "Modeling Polarized Solar Radiation from a Snow Surface for Correction of Polarization-induced Error in Satellite Data." *Journal of Quantitative Spectroscopy & Radiative Transfer* 222: 154–169. doi:10.1016/j.jqsrt.2018.10.011.
- Sun, Z. Q., Z. Y. Peng, D. Wu, and Y. F. Lv. 2018. "Photopolarimetric Properties of Leaf and Vegetation Covers over a Wide Range of Measurement Directions." *Journal of Quantitative Spectroscopy & Radiative Transfer* 206: 273–285. doi:10.1016/j.jqsrt.2017.11.017.
- Sun, Z. Q., D. Wu, Y. F. Lv, and Y. S. Zhao. 2017. "Polarized Reflectance Factors of Vegetation Covers from Laboratory and Field: A Comparison with Modeled Results." *Journal of Geophysical Research- Atmospheres* 122 (2): 1042–1065. doi:10.1002/2016jd025892.
- Tang, J., N. Zhang, D. L. Li, F. Wang, B. Z. Zhang, C. G. Wang, C. Shen, J. B. Ren, C. Y. Xue, and J. Liu. 2016. "Novel Robust Skylight Compass Method Based on Full-sky Polarization Imaging under Harsh Conditions." *Optics Express* 24 (14): 15834–15844. doi:10.1364/oe.24.015834.
- Vermote, E. F., D. Tanre, J. L. Deuze, M. Herman, and J. J. Morcrette. 1997. "Second Simulation of the Satellite Signal in the Solar Spectrum, 6S: An Overview." *IEEE Transactions on Geoscience and Remote Sensing* 35 (3): 675–686. doi:10.1109/36.581987.
- Wang, H., L. Yang, M. Zhao, D. Weibing, P. Liu, and X. Sun. 2019. "The Normalized Difference Vegetation Index and Angular Variation of Surface Spectral Polarized Reflectance Relationships: Improvements on Aerosol Remote Sensing over Land." *Earth and Space Science* 6 (6): 982–989. doi:10.1029/2019ea000593.

- Waquet, F., B. Cairns, K. Knobelspiesse, J. Chowdhary, L. D. Travis, B. Schmid, and M. I. Mishchenko. 2009. "Polarimetric Remote Sensing of Aerosols over Land." *Journal of Geophysical Research* 114 (D01206). doi:[10.1029/2008JD010619](https://doi.org/10.1029/2008JD010619).
- Xu, F., O. Dubovik, P.-W. Zhai, D. J. Diner, O. V. Kalashnikova, F. C. Seidel, P. Litvinov, et al. 2016. "Joint Retrieval of Aerosol and Water-leaving Radiance from Multispectral, Multiangular and Polarimetric Measurements over Ocean." *Atmospheric Measurement Techniques* 9 (7): 2877–2907. doi:[10.5194/amt-9-2877-2016](https://doi.org/10.5194/amt-9-2877-2016).
- Xu, X. G., and J. Wang. 2015. "Retrieval of Aerosol Microphysical Properties from AERONET Photopolarimetric Measurements: 1. Information Content Analysis." *Journal of Geophysical Research-Atmospheres* 120 (14): 7059–7078. doi:[10.1002/2015jd023108](https://doi.org/10.1002/2015jd023108).
- Yang, B., H. Zhao, and W. Chen. 2017. "Semi-empirical Models for Polarized Reflectance of Land Surfaces: Intercomparison Using Space-borne POLDER Measurements." *Journal of Quantitative Spectroscopy & Radiative Transfer* 202: 13–20. doi:[10.1016/j.jqsrt.2017.07.014](https://doi.org/10.1016/j.jqsrt.2017.07.014).
- Yang, P., Q. Feng, G. W. Gang Hong, W. J. Kattawar, M. I. Wiscombe, O. D. Mishchenko, I. Laszlo, and I. N. Sokolik. 2007. "Modeling of the Scattering and Radiative Properties of Nonspherical Dust-like Aerosols." *Journal of Aerosol Science* 38 (10): 995–1014. doi:[10.1016/j.jacros.2007.07.001](https://doi.org/10.1016/j.jacros.2007.07.001).
- Zhai, P.-W., K. Knobelspiesse, B. A. Amir Ibrahim, Y. H. Franz, M. Gao, and R. Frouin. 2017. "Water-leaving Contribution to Polarized Radiation Field over Ocean." *Optics Express* 25 (16): A689–A708. doi:[10.1364/oe.25.00a689](https://doi.org/10.1364/oe.25.00a689).
- Zhang, W. J., Y. Cao, X. Z. Zhang, and Z. J. Liu. 2015. "Sky Light Polarization Detection with Linear Polarizer Triplet in Light Field Camera Inspired by Insect Vision." *Applied Optics* 54 (30): 8962–8970. doi:[10.1364/ao.54.008962](https://doi.org/10.1364/ao.54.008962).
- Zhao, H., X. Wujian, Y. Zhang, L. Xudong, H. Zhang, J. Xuan, and B. Jia. 2018. "Polarization Patterns under Different Sky Conditions and a Navigation Method Based on the Symmetry of the AOP Map of Skyligh." *Optics Express* 26 (22): 28589–28603. doi:[10.1364/oe.26.028589](https://doi.org/10.1364/oe.26.028589).
- Zhou, G., X. Wujian, C. Niu, and H. Zhao. 2013. "The Polarization Patterns of Skylight Reflected off Wave Water Surface." *Optics Express* 21 (26): 32549–32565. doi:[10.1364/oe.21.032549](https://doi.org/10.1364/oe.21.032549).